PREDICTION OF BUBBLE SIZE DISTRIBUTIONS IN LARGE-SCALE BUBBLE COLUMNS USING COMPUTATIONAL FLUID DYNAMICS

Giorgio Besagni[a], Fabio Inzoli[a], Thomas Ziegenhein[b], Dirk Lucas[b]

[a] *Politecnico di Milano, Department of Energy*
Via Lambruschini 4a, 20156 Milan, Italy
giorgio.besagni@polimi.it and fabio.inzoli@polimi.it

[b] *Helmholtz-Zentrum Dresden-Rossendorf e. V. Institute of Fluid Dynamics*
01314 Dresden, Germany.
t.ziegenhein@hzdr.de and d.lucas@hzdr.de

ABSTRACT

A precise estimation of bubble size distributions is of fundamental and practical importance to understand the fluid dynamics and to estimate the mass transfer in bubble columns. Multiphase computational fluid dynamic simulations, in the Eulerian multi-fluid framework, are able to predict the local bubble size distributions from the fluid flow conditions by using coalescence and breakage kernels. In particular, this study concerns the prediction of the bubble size distributions in the "*pseudo-homogeneous*" flow regime, which is characterized by a wide spectrum of bubble sizes and is generally observed in industrial applications. Reliable predictions of the "*pseudo-homogeneous*" flow regime are, however, limited up to now: one important drawback concerns the selection of appropriate models for the coalescence and break-up. A set of closure relations was collected at the Helmholtz-Zentrum Dresden-Rossendorf that represents the best available knowledge and may serve as a baseline model for further investigations. In this paper, the validation of this set of closure relations has been further extended to the "*pseudo-homogeneous*" flow regime by comparing experimental and numerical bubble size distributions at different axial positions in a large-diameter and large-scale bubble column. The results have been critically analysed and may serve as basis to improve the coalescence and break-up closures.

1. INTRODUCTION

Two-phase bubble columns are widely used in the chemical, petrochemical and biochemical industries because of a number of advantages they provide in both design and operation. Unfortunately, despite the simple column arrangement, the interactions between the phases are extremely complex, making their design and scale-up very difficult (see refs. [1, 2]). The understanding of the interactions between the phases, the transport phenomena, and the global and the local fluid dynamic properties is essential to support the design and the scale-up methods [3]. In this respect, it is important to observe that the global and the local fluid

dynamic properties are related to the prevailing flow regime; in a "*large-diameter*" bubble column—accordingly with the "*large-diameter*" definition proposed by Besagni et al. [4]—the prevailing flow regimes can be distinguished into (a) the homogeneous flow regime and (b) the heterogeneous flow regime [5, 6]. In particular, the homogeneous flow regime can be distinguished into the (a) "*pure-homogeneous*" flow regime and (b) the "*pseudo-homogeneous*" flow regime, basing on the prevailing bubble size distributions: the former is characterized by a mono-dispersed BSD, whereas the latter is characterized by a poly-dispersed BSD, which is is generally observed in industrial applications. Among the fluid dynamic properties, a precise estimation of the bubble size distributions (the size distributions of the dispersed phase) is of fundamental importance to understand the fluid dynamics (i.e., owing to the stabilizing/destabilizing effect of the lift force, see ref. [5]) and to estimate the mass transfer in bubble columns. Multiphase computational fluid dynamic (CFD) simulations, in the Eulerian multi-fluid framework, are able to predict the local bubble size distributions from the fluid flow conditions using coalescence and breakage kernels. Unfortunately, reliable predictions of the "*pseudo-homogeneous*" flow regime are limited up to now: one important drawback concerns the selection of appropriate closure relations for (a) the momentum exchange between phases, (b) the effects of the dispersed bubbles on the turbulence of the continuous phase, and (c) the bubble coalescence and break-up phenomena. In a recent paper proposed by the authors [7], a CFD approach has been validated against a comprehensive dataset of local and global flow properties obtained in a "*pseudo-homogeneous*" flow regime (in the framework of a large-diameter and large-scale bubble column) [8]. In this paper, the validation of the proposed approach has been further extended and, in particular, numerical simulations have been further compared with a new experimental dataset concerning bubble size distributions at different axial and radial positions in the large-diameter and large-scale bubble column. This comparison is a further step toward a reliable tool to simulate large-scale bubble column reactors.

2. EXPERIMENTAL DATA AND METHODS

The experimental facility is a non-pressurized vertical pipe made of Plexiglas® with d_c = 0.24 m and H_c = 5.3 m. A complete description, as well as the system layout, of the facility has been presented in our previous paper (See the above-mentioned references). A pressure reducer controls the pressure upstream from the rotameters, used to measure the gas flow rate (accuracy ± 2% f.s.v., E5-2600/h, manufactured by ASA, Italy). The gas distributor is a spider-sparger distributor with hole diameters d_o = 2 - 4 mm (see, for example, refs. [5-7, 9]). The spider sparger has six arms made of 0.12 m diameter stainless steel tubes soldered to the center cylinder of the sparger. The sparger has been installed with the six holes located on the side of each arm facing upward. In our previous paper [8] we have applied a variety of experimental techniques to investigate the bubble column hydrodynamics: (a) gas holdup, (b) gas disengagement, (c) image analysis (through boxes for flow visualization (where image analysis has been applied).) and (d) optical probe measurements. The existing dataset has been extended in the recent dissertation proposed by Di Pasquali and Gottardi [10] : the image analysis, as described in our other papers, has been used to study the bubble shapes and size distributions near the sparger and in the developed region of the column; in particular, the image analysis is applied to different gas velocities in the homogeneous flow regime in both the batch and counter-current modes. In the present paper, the experimental dataset obtained at U_G = 0.0037 m/s, at different axial and radial positions, have been used to validate the numerical results.

3. PHYSICAL MODELING

3.1 The Eulerian framework

In the present study, a transient Eulerian two-fluid approach has been adopted (by using a customized CFX software). In particular, the reader may refer to the dissertation of Ziegenhein for a complete discussion concerning the Eulerian Framework [11]. In this approach the conservation equations for each phase are ensemble-averaged and the turbulence for large scale simulations is usually described with the corresponding Reynolds Averaged Navier Stokes (RANS) equations. Within such a framework, the effects of turbulence and interphase phenomena have to be taken into account using closure relations [12]: (a) the exchange of momentum between the liquid phase and gas phase, (b) the effects of the dispersed bubbles on the turbulence of the continuous phase, and (c) the processes of bubble coalescence and break-up. All of these aspects, which have been discussed in the following, have been coupled and should be considered as a whole. A set of closure relations was collected at the Helmholtz-Zentrum Dresden-Rossendorf that represents the best available knowledge [13-21] and is applied in the present paper [7].

Exchange of momentum between the liquid and gas phases. The interactions between the continuous phase and the disperse phase have been taken into account by means of source terms in the momentum equation, representing the different independent physical mechanisms: drag, lift, virtual mass, turbulent dispersion and wall lubrication forces. All the forces act together to produce observable phenomena, such as, for example, the distribution of the void fraction [22]. The list of the closure relations employed in provided in Table 1. It is worth noting that we have compared the simulations which employs the Tomiyama et al. [23] lift law with and improved lift law. Indeed, although the Tomiyama et al. [23] lift force model has been widely implemented, our experimental data [10] exibit a discrepancy with its predictions. In particular, the value of the bubble diameter at which the lift sign change occurs, appears to be overestimated by the values predicted by the Tomiyama et al. [23] law (5.80 mm); conversely, the experimental data suggest a lower value (approximately 5 mm). The source of the error has been found in the Wellek et al. [24] correlation, which links the equivalent diameter of an elliptical bubble to its major axis $d_{\perp}$. Such relationship was originally meant to describe liquid droplets moving in a liquid medium, whereas here it is used for gas bubbles. As a matter of fact, the Wellek et al. [24] correlation slightly diverges from the experimental data (As also observed in refs. [4-6, 9]). In view of this, a new correlation for $d_{\perp}$ was formulated, based on the image analysis [10]:

$$d_{\perp}[mm] = \frac{10}{3}(Eo)^{0.5} \tag{1}$$

Table 1. Closures implemented.

Force	Reference
Drag force	Ishii Zuber model [25]
Lift force	Tomiyama et al. [23]
	Modified Tomiyama et al. [23]
Turbulent dispersion force	Burns et al. [26]
Wall lubrication force	Hosokawa et al. [27]
Virtual mass force	0.5 Virtual mass coefficient

Effects of the dispersed bubbles on the turbulence of the continuous phase. This is taken into account by using the unsteady Reynolds averaged Navier Stokes equations (URANS) with the two-equation *k-ω* SST turbulence model, along with a bubble-induced turbulence contributions, as described in ref. [17].

Processes of bubble coalescence and break-up that determine the bubble size distribution. When modelling the discrete phase, one should distinguish three modelling approaches depending on the prevailing bubble sizes in the systems and the local phenomena: (a) fixed mono-dispersed approach; (b) fixed poly-dispersed approach; (c) poly-dispersed approach with bubble coalescence and break-up. Please refer to Besagni et al. [7] and Guedon et al. [28] for a comparison of these modelling approached. If coalescence and break-up cannot be neglected in the system considered (as the "*pseudo-homogeneous*" flow regime, see ref. [7]), the baseline model can be applied with the "*inhomogeneous population balance model*". In particular, the inhomogeneous multiple size group (iMUSIG) model as introduced by Krepper et al. [29] has been used. This approach splits the BSD into bubble size classes and, then, assigns the bubble size classes to different velocity groups. Each velocity group, therefore, has its own velocity field. This is important to describe effects like the bubble size-dependent movement of the gas phase caused by the lift force. In particular, two velocity groups can be assigned depending on the equivalent diameter for the change in sign of the lift force. The changes in the bubble size distributions have been given by coalescence and break-up kernels. Depending on these kernels, the changes in bubble size distributions have been modeled by changes in the bubble frequencies in the different bubble groups. The bubble coalescence and break-up modelling is a weak point in all the simulations published on bubbly flows. For this reason, Liao and Lucas reviewed all the available models [30, 31]. Then, a model combining the different mechanisms leading to bubble coalescence and break-up has been established and applied in the frame of the baseline model by Liao et al. [20]. In conclusion, this approach couples the coalescence and break-up mechanisms proposed by Liao et al. [20] in the Inhomogeneous Multiple Size Group (iMUSIG) model proposed by Krepper et al. [29]. In the present work, 2 velocity fields have been solved and 22 bubble size classes/groups represent the dispersed phase. The velocity fields have been selected accordingly with the change of sign of the lift force: a "*small*" bubble velocity field (for bubbles having a positive lift force coefficient) and a "*large*" bubble velocity field (for bubbles having a negative lift force coefficient).

3.2 The numerical settings and the numerical procedure

Three-dimensional and transient simulations have been carried out. Indeed, three-dimensional simulations have been required for accurate predictions of the gas-liquid flows in bubble columns [32-35]. The numerical simulations have been performed on a mesh of 150000 elements, where the sparger has been modeled considering a simplified three-dimensional structure: (a) the lateral arms have been simplifies as two-dimensional plains and (b) the central structure has been modelled as a cylinder. Tetra cells near the sparger and hexahedral cells in the other region of the column compose the mesh. It is worth noting that the correct modelling of the three-dimensional sparger structure is required in order to capture the structures below the sparger that may influence the bubble column fluid dynamics. For transient simulations, it must be guaranteed that the solution is independent of the time step and of the mesh size. A grid resolution study was previously conducted to ensure that convergence with respect to the spatial resolution has been achieved [28, 36]. The time discretization is characterized by using the Courant Friedrichs Lewy (*CFL*) number. In this respect, Ziegenhein et al. [13] remarked that, because the velocity is a function of position and

time so is the *CFL* number. To get a characteristic value, the root mean square of all CFL numbers in the computational domain (*RSM(CFL)*) is calculated. They concluded that *RSM(CFL) < 1* is enough for the time and space discretization. Taking into account this suggestion, in this study we have used a stricter approach: (i) *RMS*(*CFL*) < 0.50 and (ii) *CFL* < 1. Therefore, the time step is not fixed during the simulation but is increased as the flow field developed, within the two above-mentioned boundaries. The iterations within each time step have been stopped when the residuals fall below 4×10^{-5} with a minimum number of inner iterations per cycle of 4 and a maximum of 25. The numerical results compared with experimental data have been obtained as transient average over 250 s of simulation. The various numerical schemes have been chosen in order to reduce the discretization error as much as possible within the ANSYS CFX CFD code. High resolution schemes were always considered when possible in the discretization of the equation while a second order Euler backward scheme was adopted for the time discretization. Fluid properties used in the different runs of the simulations have been evaluated at the column mid-point.

3.3 Initial and boundary conditions

In the present paper, we have compared the experimental and numerical results obtained at U_G = 0.0037 m/s (please refer to ref. [10] for the complete dataset employed). Mass flow inlet boundary conditions have been assigned at the air distributor using source points located in the same position as the distributor holes (Figure 1). For each operating condition analysed, the source point activation has been selected consistently to what was observed in the experimental setup on the basis of the visual observation. Indeed, the source points have been activated (and the corresponding mass flow rate has been seleted) based on visual observation, in order to take into account the maldistribution at the gas sparger. Please refer to our previous paper for the description of the gas maldistribution. Table 2 present the size groups at the different source points, used as inlet conditions. Each size group for the gas phases has been computed based on image analysis of the gas sparger phenomena: first, an image analysis was performed and, subsequently, the bubble size distributions obtained were approximated by log-normal distributions. Hence, the number of lognormal distributions necessary to run a single case is seven, as a radial symmetry has been assumed. Degassing boundary condition has been assigned at the outlet. At the walls, a no-slip boundary condition has been applied for the continuous phase and a free slip condition for the disperse phase.

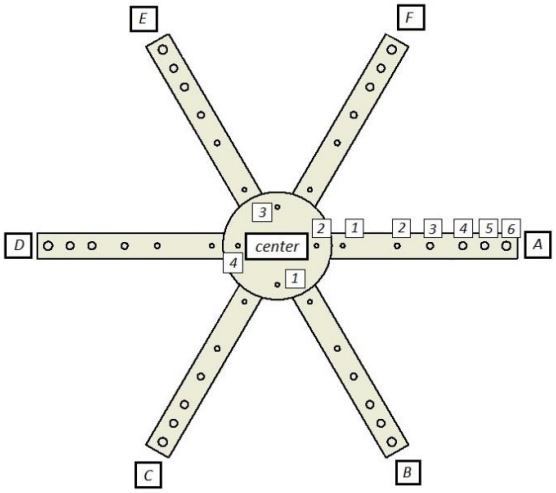

Figure 1. Holes identification used for the input setup of numerical simulations.

Table 2. Velocity and Size Groups used as input for the simulations.

Velocity Group	Size Group diameter [mm]	Hole 0	Hole 1	Hole 2	Hole 3	Hole 4	Hole 5	Hole 6
"Small-bubble"	1	0.0000	0.0000	0.0000	0.0000	0.0000	0.0000	0.0000
	2	0.0000	0.0000	0.0000	0.0000	0.0000	0.0026	0.0000
	3	0.0002	0.0056	0.0035	0.0018	0.0006	0.0442	0.0015
	4	0.0364	0.1477	0.1023	0.0774	0.0485	0.2385	0.0718
	5	0.9634	0.8467	0.8942	0.9207	0.9509	0.7147	0.9267
"Large-bubbles"	6	0.0022	0.1941	0.0084	0.0022	0.0011	0.0121	0.0021
	7	0.0100	0.2514	0.0223	0.0073	0.0049	0.0207	0.0072
	8	0.0281	0.2241	0.0428	0.0172	0.0137	0.0306	0.0175
	9	0.0559	0.1555	0.0657	0.0319	0.0288	0.0407	0.0329
	10	0.1294	0.1127	0.1244	0.0745	0.0742	0.0728	0.0772
	12	0.2452	0.0504	0.2081	0.1603	0.1712	0.1299	0.1661
	14	0.2243	0.0098	0.1901	0.1891	0.2050	0.1460	0.1935
	16	0.1537	0.0017	0.1444	0.1800	0.1892	0.1498	0.1806
	18	0.0873	0.0003	0.0973	0.1486	0.1468	0.1444	0.1454
	20	0.0437	0.0000	0.0607	0.1112	0.1011	0.1334	0.1058
	22	0.0201	0.0000	0.0359	0.0777	0.0640	0.1196	0.0718

3.6 Post-Processing

The numerical and the experimental bubble size distributions (in terms of relative frequency distributions and size fraction distributions, see ref. [7]) have bene compared. The experimental data have been obtained by image analysis (i.e., sampling bubbles from images). Therefore, the experimental results represent a zonal average, rather than single point variables, as the ones available from the computer-based simulations. In this respect, in order to compare the experimental and the numerical results, the mesh node-based data from the simulations have to be carefully averaged over the all nodes belonging to specific mesh zones. These zones have to be representative of the location from which the real bubbles were sampled, i.e. at the wall and the centre section of the column at different heights. Regarding the wall section, the zone of the mesh where the results have been averaged in a volume with a circular crown shaped base, included an angle of 90° and a height of 0.2 m. The thickness of the base has been selected at a value of 0.022 m which is half of the focal depth of the camera used for the image analysis. The selection of this value is related back to the sampling technique, according to which the sampled bubbles have been chosen by their degree of sharpness. Concerning the central section, instead, the averaging zone is a parallelepiped whit a height of 0.2 m, a base of 0.17 m and a depth equal to 0.044 m, which is, this time, the whole depth of field of the camera. A visual representation of such averaging zones has been shown in Figure 2.

.

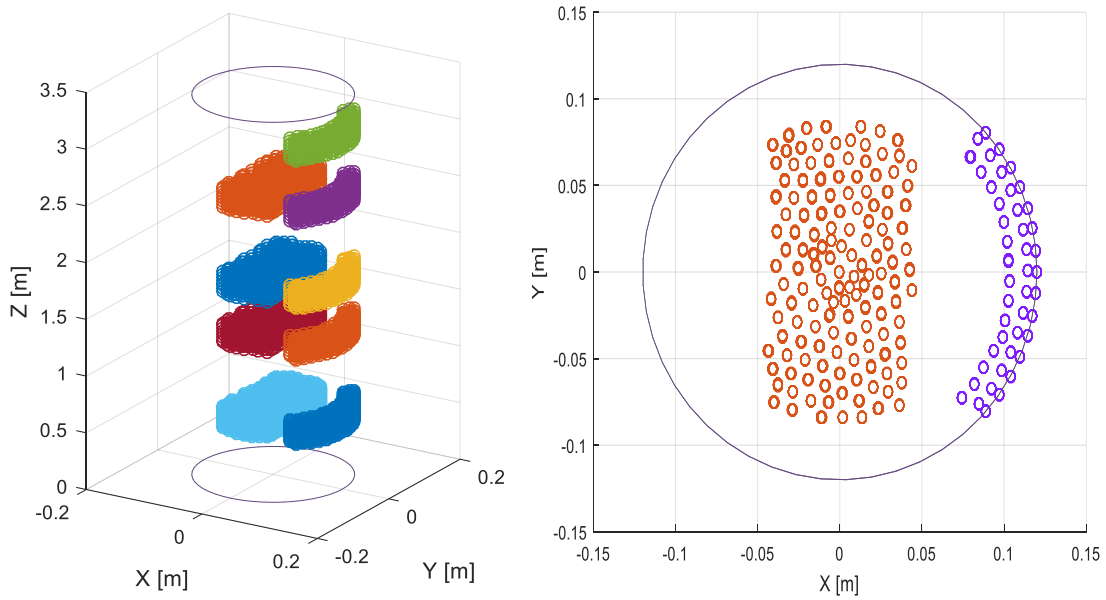

Figure 2. Averaging mesh zones.

4. RESULTS AND DISCUSSION

Figure 3 and Figure 4 display the experimental and numerical bubble size distributions: the system is poly-dispersed in nature and the present homogeneous flow regime is classified as "*pseudo-homogeneous*" flow regime. In particular, Figure 3 and Figure 4 display the axial evolution for the bubble size distributions at the center and near the wall of the bubble column, respectively. The mean diameter of the distribution is approximately 2 mm in the developing region and it is approximately 4 mm in the developed one. These values are in agreement with the results of Lau et al [37], even if the experimental setup is slightly different. From these experimental results it is clear that the coalescence and break-up phenomena are not negligible, thus supporting the speculations in ref. [7]. Moreover, comparison figure 3 and Figure 4, it is obvious that bubble at wall are on average smaller than the ones in the center section (the mean diameter at wall and center are about 3 and 4 mm, respectively): the large bubbles, having a negative lift coefficient, tend to migrate from the low liquid velocity region towards the high liquid velocity regions (Lucas et al., 2005; Tomiyama et al., 2002): in the batch mode, the larger bubbles tend to migrate toward the center of the column. It is worth noting the different shape of the near-wall and center bubble size distributions: the ones related to the wall of the columns have a very small variance if compared to the ones at the center, namely the center bubble size distributions are much more spread out on the whole diameters range with respect to the wall. This result supports the fact that the bubbles in the center section are larger than the ones at wall. This result is observed at every vertical coordinate analyzed in this work. The only exceptions are the first axial positions (approximately 0.3 m above the distributor itself), where the bubble distribution at the center has smaller mean diameter than the one at wall. One possible explanation for that is that the flow rate exiting the sparger is highest in the column center region.

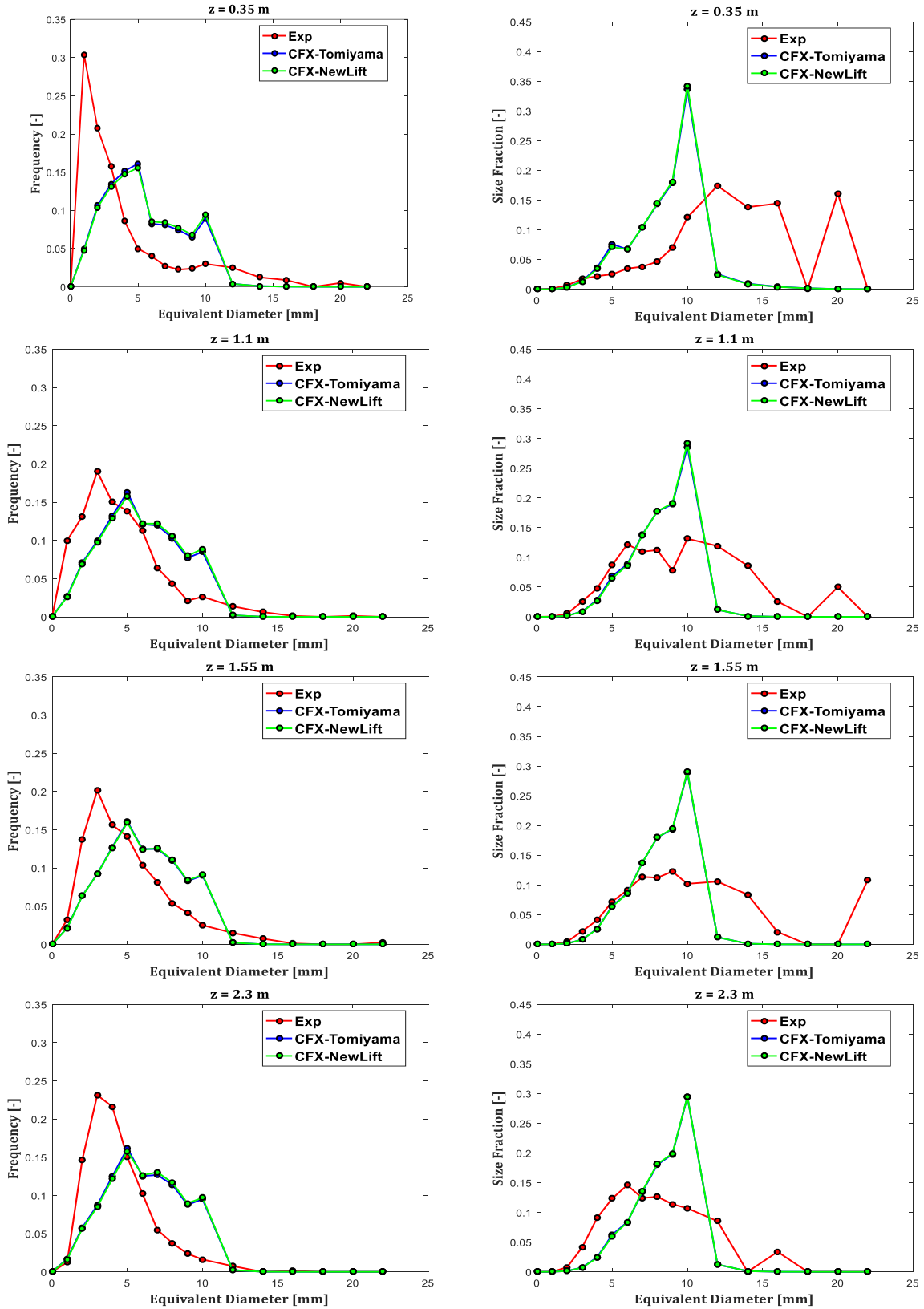

Figure 3. Simulation results: size fractions and BSD at the center section

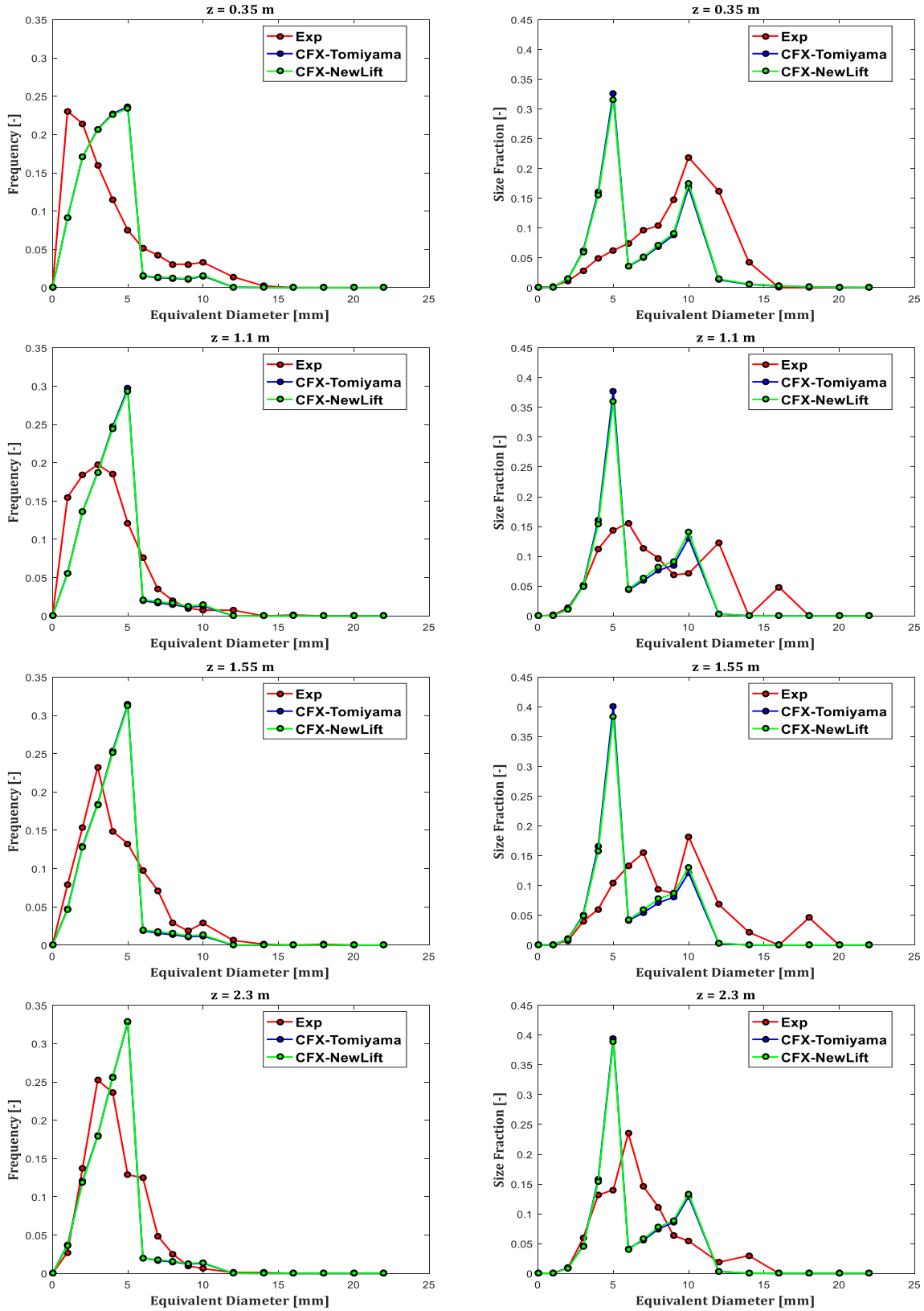

Figure 4. Simulation results: size fractions and BSD at the wall section

Figure 3 and 4 also compares the outcomes of the simulations at U_G=0.0037 m/s, set both with the Tomiyama and corrected lift model, with the experimental data, in terms of bubble diameter BSDs and size fractions. Generally, considering the state-of-the-art in two-phase population balance modelling, the present numerical results are very promising. It is worth noting that the modified lift force does not seem to have a considerable influence over the results. If looking closer the experimental and the numerical results, it is clear that the CFD result overestimates the contribution of the bubbles belonging to the fifth size group, corresponding to a mean diameter of 5mm, at the wall. The above-mentioned overestimation of the fifth size group, results in an over predicted peak. Therefore, huge bubbles are present in that part of the column, and breakup will be stronger and more frequent there. Probably that is a region where breakup has just occurred and small bubbles formed that have been subjected to Tomiyama lift force still have to migrate towards the wall section. Moreover, the *CFX* model does not predict the larger bubbles, present in the largest size groups, whereas the experimental observations indicated the presence of such larger bubbles, especially at the center region. These large deformed bubbles are very important because of their large volume and they significantly affect the flow field of both phases. Nevertheless, the population balance model used for the calculations considers such structures as large and unstable bubbles, which have been consequently destroyed due to breakup. Another important remark is that both the numerical BSD and size fraction profiles significantly change mainly in the first and second position from the bottom; above this region they tend to stabilize. This result was somehow expected because the CFD model does not account for disequilibrium due to the sudden coalescence and the formation of unstable gas structures: once the prevailing bubble size distribution reaches the equilibrium, it does not changes anymore.

4. CONCLUSIONS

This study concerns the prediction of the bubble size distributions in the "*pseudo-homogeneous*" flow regime, which is characterized by a wide spectrum of bubble sizes and is generally observed in industrial applications. In particular, this study aims to extent the validation of a previously proposed approach to propose a further step towards the simulation of large-scale bubble column reactors and provide clear guidelines to simulate industrial scale reactors, within the boundaries of the "*pseudo-homogeneous*" flow regime. In particular, in this paper the validation of a previously proposed approach has been extended to by comparing experimental and numerical bubble size distributions at different axial positions in a large-diameter and large-scale bubble column. In addition, a modified lift force law has been proposed and implemented. The results have been critically analysed and may serve as basis to improve the coalescence and break-up closures. The numerical results approximate the experimental data fairly well, considered the complexity of the problem and the simplicity of the Euler-Euler approach that was used. Tuning the breakup and coalescence model coefficients may create better results concerning this specific study, whilst a general improvement valid for any experimental and industrial setup would require a much deeper study to be declared feasible within the Euler-Euler framework. The present results will be extended to consider additional operating conditions.

REFERENCES

[1] P. Rollbusch, M. Bothe, M. Becker, M. Ludwig, M. Grünewald, M. Schlüter, R. Franke, Bubble columns operated under industrially relevant conditions – Current understanding of design parameters, Chemical Engineering Science, 126 (2015) 660-678.
[2] C. Leonard, J.H. Ferrasse, O. Boutin, S. Lefevre, A. Viand, Bubble column reactors for high pressures and high temperatures operation, Chemical Engineering Research and Design, 100 (2015) 391-421.
[3] A. Shaikh, M. Al-Dahhan, Scale-up of Bubble Column Reactors: A Review of Current State-of-the-Art, Industrial & Engineering Chemistry Research, 52 (2013) 8091-8108.
[4] G. Besagni, P. Brazzale, A. Fiocca, F. Inzoli, Estimation of bubble size distributions and shapes in two-phase bubble column using image analysis and optical probes, Flow Measurement and Instrumentation, 52 (2016) 190-207.
[5] G. Besagni, F. Inzoli, G. De Guido, L.A. Pellegrini, The dual effect of viscosity on bubble column hydrodynamics, Chemical Engineering Science, 158 (2017) 509-538.
[6] G. Besagni, F. Inzoli, The effect of liquid phase properties on bubble column fluid dynamics: Gas holdup, flow regime transition, bubble size distributions and shapes, interfacial areas and foaming phenomena, Chemical Engineering Science, In Press (2017).
[7] G. Besagni, F. Inzoli, T. Ziegenhein, D. Lucas, Computational Fluid-Dynamic modeling of the pseudo-homogeneous flow regime in large-scale bubble columns, Chemical Engineering Science, 160 (2017) 144-160.
[8] G. Besagni, F. Inzoli, Comprehensive experimental investigation of counter-current bubble column hydrodynamics: holdup, flow regime transition, bubble size distributions and local flow properties, Chemical Engineering Science, 146 (2016) 259–290.
[9] G. Besagni, F. Inzoli, Bubble size distributions and shapes in annular gap bubble column, Experimental Thermal and Fluid Science, 74 (2016) 27-48.
[10] A. Di Pasquali, E. Gottardi, Experimental and numerical investigation of a large-scale bubble column: scale-up criteria and influence of liquid properties, in, Vol. M.S. Degree, Politecnico di Milano, 2016.
[11] T. Ziegenhein, Fluid dynamics of bubbly flows, in, Technische Universität Berlin, 2016.
[12] M. Ishii, T. Hibiki, Thermo-Fluid Dynamics of Two-Phase Flow, Springer-Verlag New York, 2011.
[13] T. Ziegenhein, R. Rzehak, D. Lucas, Transient simulation for large scale flow in bubble columns, Chemical Engineering Science, 122 (2015) 1-13.
[14] T. Ziegenhein, D. Lucas, R. Rzehak, E. Krepper, Closure relations for CFD simulation of bubble columns, in: 8th International Conference on Multiphase Flow. ICMF 2013, , Jeju (Korea), 2013.
[15] R. Rzehak, S. Kriebitzsch, Multiphase CFD-simulation of bubbly pipe flow: A code comparison, International Journal of Multiphase Flow, 68 (2015) 135-152.
[16] R. Rzehak, E. Krepper, C. Lifante, Comparative study of wall-force models for the simulation of bubbly flows, Nuclear Engineering and Design, 253 (2012) 41-49.
[17] R. Rzehak, E. Krepper, Y. Liao, T. Ziegenhein, S. Kriebitzsch, D. Lucas, Baseline Model for the Simulation of Bubbly Flows, Chemical Engineering & Technology, 38 (2015) 1972-1978.
[18] R. Rzehak, E. Krepper, Closure models for turbulent bubbly flows: A CFD study, Nuclear Engineering and Design, 265 (2013) 701-711.
[19] D. Lucas, R. Rzehak, E. Krepper, T. Ziegenhein, Y. Liao, S. Kriebitzsch, P. Apanasevich, A strategy for the qualification of multi-fluid approacheds for nuclear reactor safety, Nuclear Engineering and Design, 299 (2016) 2–11.

[20] Y. Liao, R. Rzehak, D. Lucas, E. Krepper, Baseline closure model for dispersed bubbly flow: Bubble coalescence and breakup, Chemical Engineering Science, 122 (2015) 336-349.
[21] J. Liao, T. Ziegenhein, R. Rzehak, Bubbly flow in an airlift column: a CFD study, Journal of Chemical Technology & Biotechnology, (2016) n/a-n/a.
[22] M. Pourtousi, J.N. Sahu, P. Ganesan, Effect of interfacial forces and turbulence models on predicting flow pattern inside the bubble column, Chemical Engineering and Processing: Process Intensification, 75 (2014) 38-47.
[23] A. Tomiyama, H. Tamai, I. Zun, S. Hosokawa, Transverse migration of single bubbles in simple shear flows, Chemical Engineering Science, 57 (2002) 1849-1858.
[24] R.M. Wellek, A.K. Agrawal, A.H.P. Skelland, Shape of liquid drops moving in liquid media, AIChE Journal, 12 (1966) 854-862.
[25] M. Ishii, N. Zuber, Drag coefficient and relative velocity in bubbly, droplet or particulate flows, AIChE Journal, 25 (1979) 843-855.
[26] A.D. Burns, T. Frank, I. Hamill, J.-M. Shi, The Favre averaged drag model for turbulent dispersion in Eulerian multi-phase flows, in: 5th international conference on multiphase flow, ICMF, Vol. 4, 2004, pp. 1-17.
[27] S. Hosokawa, A. Tomiyama, S. Misaki, T. Hamada, Lateral migration of single bubbles due to the presence of wall, in: ASME 2002 Joint US-European Fluids Engineering Division Conference, American Society of Mechanical Engineers, 2002, pp. 855-860.
[28] G.R. Guédon, G. Besagni, F. Inzoli, Prediction of gas–liquid flow in an annular gap bubble column using a bi-dispersed Eulerian model, Chemical Engineering Science, 161 (2017) 138-150.
[29] E. Krepper, D. Lucas, T. Frank, H.-M. Prasser, P.J. Zwart, The inhomogeneous MUSIG model for the simulation of polydispersed flows, Nuclear Engineering and Design, 238 (2008) 1690-1702.
[30] Y. Liao, D. Lucas, A literature review on mechanisms and models for the coalescence process of fluid particles, Chemical Engineering Science, 65 (2010) 2851-2864.
[31] Y. Liao, D. Lucas, A literature review of theoretical models for drop and bubble breakup in turbulent dispersions, Chemical Engineering Science, 64 (2009) 3389-3406.
[32] D. Pfleger, S. Gomes, N. Gilbert, H.G. Wagner, Hydrodynamic simulations of laboratory scale bubble columns fundamental studies of the Eulerian–Eulerian modelling approach, Chemical Engineering Science, 54 (1999) 5091-5099.
[33] A. Sokolichin, G. Eigenberger, Applicability of the standard k–ε turbulence model to the dynamic simulation of bubble columns: Part I. Detailed numerical simulations, Chemical Engineering Science, 54 (1999) 2273-2284.
[34] R.F. Mudde, O. Simonin, Two- and three-dimensional simulations of a bubble plume using a two-fluid model, Chemical Engineering Science, 54 (1999) 5061-5069.
[35] K. Ekambara, M.T. Dhotre, J.B. Joshi, CFD simulations of bubble column reactors: 1D, 2D and 3D approach, Chemical Engineering Science, 60 (2005) 6733-6746.
[36] G. Besagni, Bubble column fluid dynamics: experimental and numerical investigations, in, Vol. Ph.D, Politecnico di Milano, 2016.
[37] Y. Lau, K.T. Sujatha, M. Gaeini, N. Deen, J. Kuipers, Experimental study of the bubble size distribution in a pseudo-2D bubble column, Chemical Engineering Science, 98 (2013) 203-211.